Design of an acoustic metamaterial lens using genetic algorithms

Dennis Li, Lucian Zigoneanu, Bogdan-Ioan Popa, and Steven A. Cummer[a)]
Department of Electrical and Computer Engineering, Duke University, Durham, North Carolina 27708

(Received 29 November 2011; revised 24 May 2012; accepted 31 May 2012)

The present work demonstrates a genetic algorithm approach to optimizing the effective material parameters of an acoustic metamaterial. The target device is an acoustic gradient index (GRIN) lens in air, which ideally possesses a maximized index of refraction, minimized frequency dependence of the material properties, and minimized acoustic impedance mismatch. Applying this algorithm results in complex designs with certain common features, and effective material properties that are better than those present in previous designs. After modifying the optimized unit cell designs to make them suitable for fabrication, a two-dimensional lens was built and experimentally tested. Its performance was in good agreement with simulations. Overall, the optimization approach was able to improve the refractive index but at the cost of increased frequency dependence. The optimal solutions found by the algorithm provide a numerical description of how the material parameters compete with one another and thus describes the level of performance achievable in the GRIN lens. © *2012 Acoustical Society of America*. [http://dx.doi.org/10.1121/1.4744942]

PACS number(s): 43.60.Fg, 43.60.Lq, 43.20.El, 43.20.Bi [ANN] Pages: 2823–2833

I. INTRODUCTION

Composite acoustic metamaterials are engineered in a complex fashion through structured, subwavelength-scale unit cells to produce specific effective materials, which have enabled a range of novel acoustic devices to expand.[1–11] One application of acoustic metamaterials being aggressively pursued at the present is acoustic lenses for imaging applications. By spatially varying the effective refractive index in the acoustic metamaterial, one can create a gradient refractive index (GRIN) lens with flat and relatively thin geometry. It has already been shown that a medium in which the refractive index varies orthogonally to the optical axis can serve as an effective focusing lens.[12] These design techniques have been adopted in acoustics to realize sonic lenses in several forms.[10,11] Initially implemented as dispersive arrangements of cylindrical rods,[10] it has since been demonstrated that sonic lenses composed of more complex metamaterial unit cells[11] can result in improved performance.

Typically, good imaging systems require broadband lenses that possess small focal lengths and minimal reflection. In this work, we address the challenge of designing the metamaterial unit cells to construct such a lens by numerically optimizing the geometry of each unit cell structure of the GRIN lens. Within this context of a GRIN unit cell approach to constructing lenses, there is no neat description or table of values showing how these values relate to one another, e.g., the maximum achievable refractive index and bandwidth given an impedance of 2.0. An optimization procedure that can characterize this relationship is very useful and would be very helpful not just for acoustic lenses, but also any acoustic metamaterial.

Several types of optimization algorithms have been previously employed in the design of metamaterial-based devices in both acoustic and electromagnetic regimes.[13,14] Here, we use genetic algorithms (GAs). GAs are well equipped to this task of shape optimization and have historically been reliable, with frequent application to electromagnetism.[15]

GAs have also been applied to acoustic lens design before, but through a phononic crystal approach based on scattering patterns.[16] The purpose was to optimize on the device level by finding a distribution of cylinders for which the focusing spot was best defined. A secondary purpose includes some bandwidth optimization as well, but no attention has been given to other important lens properties such as aberrations, or impedance mismatch.

In contrast, the approach employed here attempts to design on the unit cell level rather than the device level because this decomposes the complex problem of lens design into easier to solve sub-tasks. In order to accomplish this, the refractive index profile of the lens follows a predetermined distribution like in Ref. 11. The performance of the lens is then determined by its maximum refractive index (located at the center of the lens), impedance mismatch, and bandwidth.

Thus, the goal becomes one of designing unit cell structures to increase the maximum refractive index, to reduce the impedance mismatch and to increase the bandwidth of the lens. This is a typical optimization problem that requires finding an acceptable trade-off between these parameters. For example, increasing the refractive index will either increase the impedance (because more dense material is used) and/or decrease the bandwidth (by operating closer to the unit cell resonant frequency).

To demonstrate the design results, we fabricate a lens constructed from the optimized unit cell structures and test its performance as a collimator.

II. SIMULATION METHODS

A. Unit cell and lens design

A GRIN lens is characterized by a refractive index distribution that is minimum near the edges of the lens and

[a)]Author to whom correspondence should be addressed. Electronic mail: cummer@ee.duke.edu

maximum at the center of the lens (in the direction orthogonal to the acoustic axis). In this GRIN lens design scheme, as the maximum refractive index increases, the focal distance decreases. This allows for thinner lenses that can achieve the same focal distance with less impedance mismatch and fewer materials.[10–12] Here, a hyperbolic secant distribution is imposed because it produces lenses free of aberrations [see Fig. 1(a)].[11] This distribution is approximated by discrete unit cells, each corresponding to some specific refractive index [see Fig. 1(b)].

Each unit cell consists of a solid structure in an air background. The unit cells were always fixed in size at approximately one-tenth the operating wavelength in air to force homogeneity and have 45° rotational symmetry to force isotropy, following approaches in Ref. 11. In order to achieve the refractive index distribution, the internal structures of unit cells (the unit cells were constant in size) outside of the center were shrunk until they achieved their specified refractive index.[8,11]

Henceforth in this paper, the term unit cell will refer to the unit cell at the center of the lens unless specified otherwise (e.g., the unit cell with the maximum refractive index in the lens). The GA is concerned with only optimizing the internal structure of this center unit cell.

An underlying assumption present in this paper is that each unit cell is characterized with its own effective material parameters, independent of other unit cells. Otherwise, it would become a very complex problem to determine how the refractive index of each unit cell changes when it is placed inside a lens and then account for that accordingly. Moreover, running any sort of optimization algorithm would be extremely difficult because every simulation would be extremely computationally expensive if each simulation consisted of arrays of unit cells.

Theoretical justification is provided in Refs. 8 and 17 and used in Ref. 11. Figure 2 exemplifies this approach on a randomly generated unit cell used in the initial steps of the GA. Briefly summarized, each unit cell is individually simulated inside the center of a waveguide four times longer than the unit cell side length, with sound hard walls parallel to the acoustic axis. A plane wave is sent parallel to the acoustic axis, and the reflection and transmission coefficients are computed. Inversion operations are performed on these coefficients to obtain the refractive index and impedance of each unit cell.

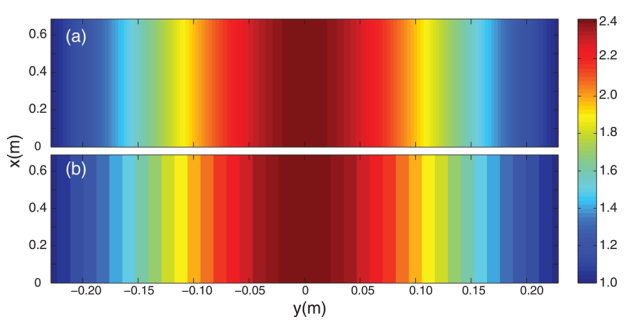

FIG. 1. (Color online) Temperature map of the hyperbolic secant refractive index profile within a GRIN lens. (a) Continuous lens, (b) discrete unit cell lens.

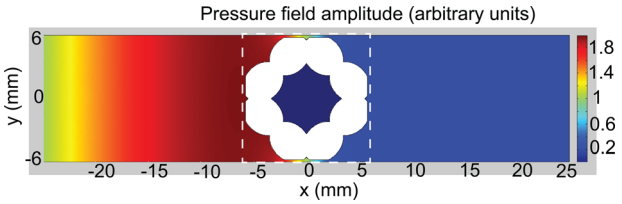

FIG. 2. (Color online) Randomly selected unit cell generated in the zeroth generation using the shape generation algorithm and analyzed at 3000 Hz. The cell boundaries are marked by the dashed square. Note that the top and bottom boundaries are rigid (sound hard) and the acoustic wave is propagating from left to right.

Using sound hard walls simulates an infinite array of identical unit cells perpendicular to the acoustic axis.[8,17] In the direction parallel to the acoustic axis, one might expect the material parameters to change because of influence from neighboring unit cells. However, as shown in Ref. 8, this influence is negligible. Hence, the simulation configuration used works quite well as an approximation to deriving the effective material parameters of each unit cell.

Note that there is a gap present between the unit cell structure and the hard walls of the waveguide. This was forced in order to ensure that they did not touch since this simulation approximation assumed distinct unit cells. Because of fabrication issues described in more detail in Sec. IV A, this gap size was set to 0.2 mm. The operating frequency used for simulation and design was 3000 Hz, corresponding to a wavelength of 114 mm in air. Therefore, the corresponding unit cell size is a square of side length 12 mm. In simulation, the internal structures of the unit cells are modeled as elastic solids with a density of 7850 kg/m^3, a Poisson ratio of 0.33, and a Young's modulus of 2.0×10^{11} Pa. The background medium was air with a density of 1.28 kg/m^3 and a speed of sound of 343 m/s.

B. Physical constraints

The three parameters of interest (refractive index, impedance, and bandwidth) are competing variables. This means, for instance, that attempting to maximize the refractive index will inherently cause a trade-off with the other two variables. This follows from $Z = nB$, where B is the bulk modulus, and $\lambda = \lambda_{\text{air}}/n$ (see Ref. 8 for a more detailed explanation). Increasing the refractive index requires either adding additional mass and increasing the bulk modulus, or decreasing the bandwidth by shifting the resonance frequency toward the operating frequency.

It is unknown to what extent one parameter can be optimized without causing a noticeable trade-off in the other two. The optimization procedure thus does not employ any upper bounds or target values during the optimization of these variables, and instead allows them to compete with one another and settle on an acceptable trade-off. (An example of a non-acceptable trade-off would be a unit cell characterized by a bandwidth of only 3000 Hz ± 50 Hz or an impedance of five would not be reasonable for use even if it had a very large refractive index.)

The unit cells were also designed to operate on a regime where the unit cell is small relative to the effective

wavelength. If the metamaterial operates outside of this frequency range, then its material parameters become much more frequency dependent and inconsistent.[8]

C. GA

The unit cell structure can take on a nearly infinite number of different shapes, which makes it very difficult to apply an exhaustive search to the task of shape optimization. For instance, if the unit cell were to be discretized into a 16 by 16 pixel box where square columns could be placed, there would be 256 choose K different possible combinations, where K is the number of columns. In this work, we employ a continuous distribution of more complex "subshapes," which can be oriented and placed continuously, rather than discrete square columns, which makes the search space extremely large. Therefore, global search algorithms that more intelligently search for the optimal solution within the search space are used.

GAs fall within the class of metaheuristic algorithm that work by iteratively improving themselves with past data after each iteration rather than performing a stochastic or exhaustive search. This results in a more computationally manageable algorithm that still thoroughly explores the search space.[15,19] A practical benefit of this approach is that it is extremely easy to parallelize the algorithm since the calculations (individuals) of each iteration (generation) are independent of one another.

Inspired by the processes of natural selection and genetics, GAs create "environments" where the most fit individuals tend to pass on their data (genes) to the next generation. Over time, the performance of the population should then increase. In this work, each individual is a unit cell whose structure is represented by its chromosome. The algorithm then selects the most fit unit cell designs and performs the operations of crossover and mutation on their chromosomes to generate the child population. A brief summary of the process is shown in Fig. 3 and described in more detail in the following sections.

The GA begins with some initial population size and other various parameters such as mutation rate. The initial population is generated. For every generation following, the individuals are ranked based on fitness to find the survivors who then mate to create the next generation. This process is repeated until the solution converges.

1. Shape generation

For the final metamaterial lens to approximate a continuous GRIN lens, the unit cells must appear homogeneous and isotropic to the incoming acoustic wave. Homogeneity is ensured by setting the unit cell to be ten times smaller than the wavelength in air. Isotropy is approximated by forcing 45° rotational symmetry.[18]

In order to force this symmetry, the following algorithm is employed. First, some structure is generated within a right triangular region in the first quadrant of a Cartesian plane. This region is then duplicated, flipped across the line $y=x$, and merged with the previous region. This process is repeated over the y axis and the x axis to create the final unit cell shape design that is symmetric (see Fig. 4).

The structure that occupies the triangular region is generated by the composition of up to 18 subshapes; 18 was chosen as the maximum number of subshapes in order to reduce computational strain while still maintaining a broad search space. Each subshape was either a parallelogram or ellipse because these two shapes can both be easily described by the same set of parameters (semi major/minor axis, position, rotation). The subshapes would then be either "added" or "subtracted" from the current structure.

Each subshape was assigned two values for dimensions, two values for position, one value for the angle of rotation, one flag for shape type, and one flag for "add" or "subtract." The position was based on the center of the shape and had to have some overlap with the triangle region [see Fig. 4(b)]. The angle of rotation was a random value between 0° and 180°. An example of a unit cell structure generated with the shape generation algorithm is shown in Fig. 2.

2. Chromosome design

The method of subshapes was preferred because it is advantageous in chromosome design. An alternative approach to building the structure for instance could have been to generate random points and then to connect them via nonintersecting curved or straight edges to form volumes. This approach probably would have resulted in even more structural variation, but is hardly usable in a GA where this structure must be easily manipulated. For instance, performing a crossover operation where the structure of two parents must be combined would have been very difficult (see Sec. II C 5). The operation would have to be able to pick the points and edges properly to ensure that the edges of the child do not intersect but still somehow retain a similar form to those of its parents. Thus, there was a significant design challenge in the chromosome as well.

Having already partially described the subshape methodology in Sec. II C 1 it is straightforward to implement the rest of the chromosome design. Every subshape is represented as a "gene," a vector of the values describing a subshape. Each chromosome is a collection of these genes as a list, serving as a textual representation of the internal structure of some unit cell (see Table I).

In the initial population, there were 80 individuals, or chromosomes. This number was chosen because a population size between 50 and 100 improved long-term performance.[19] Each chromosome was then assigned a random number of genes, between 1 and 18. By varying the number of genes per chromosome, variation in the final unit cell structure included both "simple" and "complex" structures. This was also necessary so that the number of genes could vary in future generations where the chromosomes are generated through crossover. Otherwise, the only way the number of genes would change would be through the mutation operator.

3. Selection

The most popular methods of selection in GA literature are roulette wheel, tournament selection, and Pareto

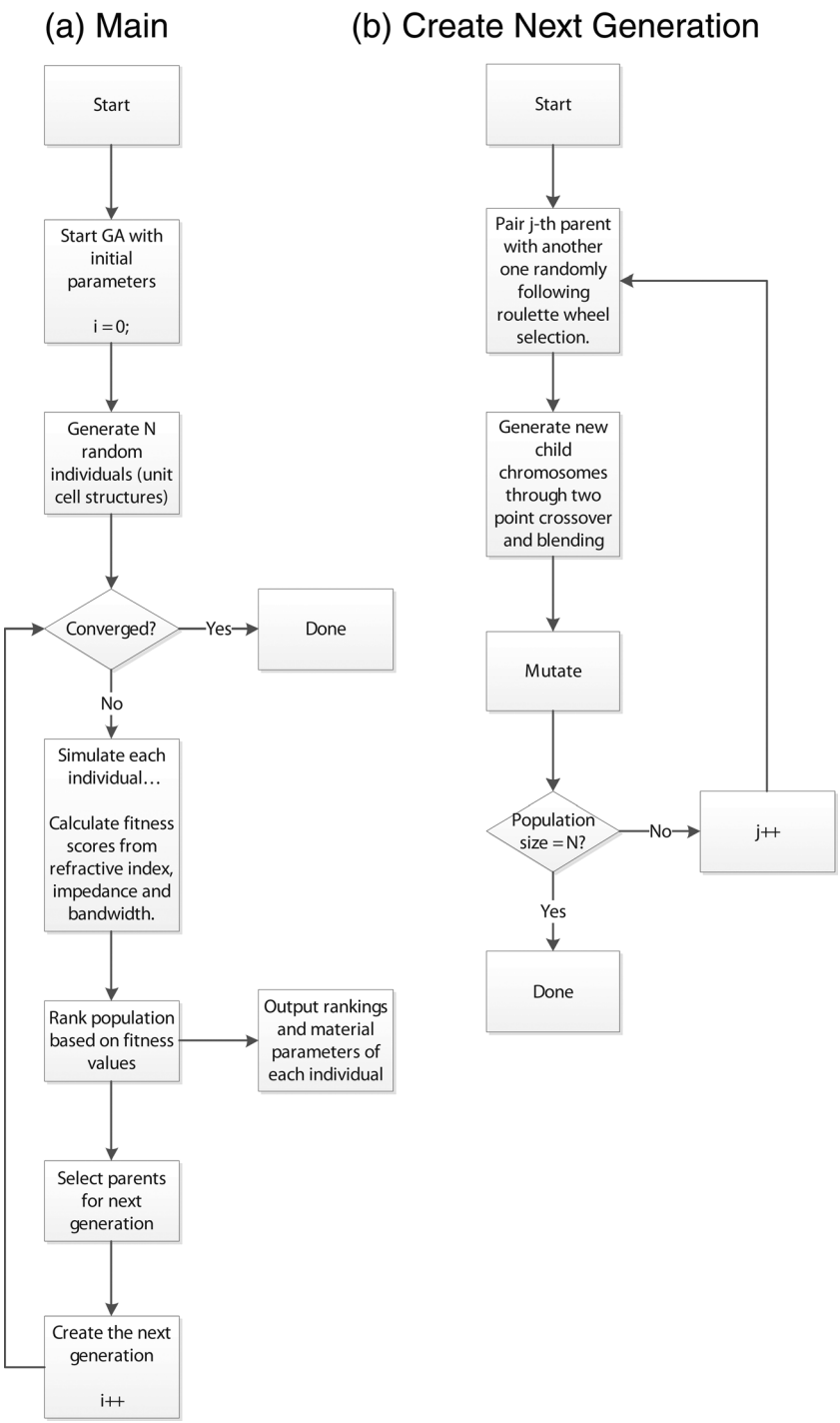

FIG. 3. Flowcharts describing the logical implementations of (a) main genetic algorithm function and (b) the subroutine to create the new generations.

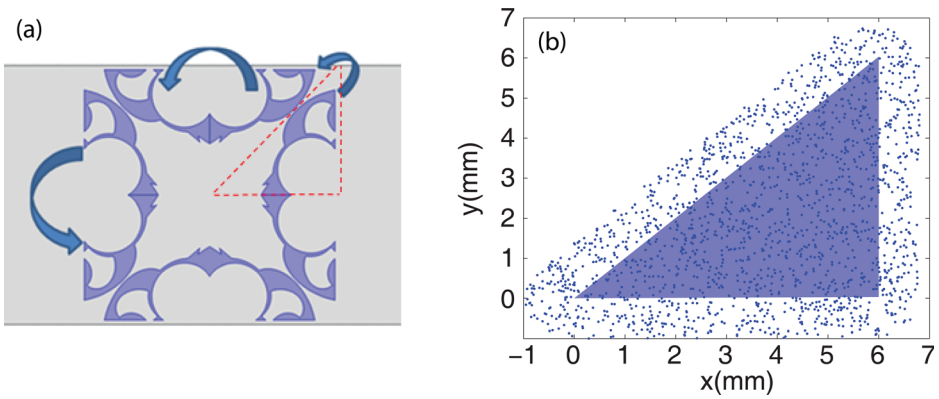

FIG. 4. (Color online) Unit cell generation. (a) Unit cell structures for the bottom half of the first quadrant (highlighted by the dashed triangle) are generated first. This region is then duplicated and flipped over the $y = x$ line and merged with the original structure. This process is repeated over the y axis and the x axis. (b) Scatter plot of generated positions of the subshape. The distribution is largely uniform so that no particular shape configuration is preferred.

TABLE I. Array visualization of the chromosome.[a]

Gene	x	y	θ	C	d	Subshape type	Add/sub
0	1.5	−1.44	76.7	1.99	1.98	0	1
1	2.72	1.6	101.4	7.9	1.7	0	1
2	6.53	1.73	40.6	1.34	1.03	1	0
3							
4	0.31	−0.026	50.6	2.13	0.69	0	0
5							
6	2.3	−1.49	10.2	2.33	1.22	1	1
7	1.7	0.107	92.4	1.95	0.26	0	0
8							
9	5.55	2.52	108.5	0.14	2.17	1	0
10	4.76	2.88	87.5	0.45	1.13	1	0
11							
12	4.55	2.91	63.4	2.35	0.89	0	0
13	5.16	4.84	144	2.32	1.02	0	1
14	3.87	5.86	164.4	1.29	1.81	0	1
15							
16							
17							

[a]Each row is a "gene," a vector representation of a subshape. A flag of 0 for subshape type represents a parallelogram, while 1 represents ellipses. An add/sub value of 0 represents addition and 1 represents the subtract operator. Blank spaces mean that no subshape is present at that index (e.g., at least one of the parents had no gene at that location or a mutation had removed it). For instance, the gene at index 0 corresponds to a parallelogram with its center at (1.507, −1.44 mm), rotated by 76.74° with an initial horizontal semiaxis value of 1.996 mm and an initial vertical semiaxis value of 1.982 mm. This shape is to be subtracted from what was previously there. In this case, since there is nothing it is effectively a null gene, like gene 3 or 5.

optimization. Roulette wheel (fitness proportionate selection) is the simplest of them to implement and is used in this paper. Tournament selection tends to be more popular, but numerical testing demonstrates that it has no significant benefits over roulette selection.[19] Pareto optimization works well with multidimensional optimization by creating a surface of the optimal solutions across n-dimensions, but requires a very large population size, which is computationally expensive.[19] In roulette wheel selection the probability that an individual survives is directly proportional to its performance.

When choosing individuals for the next generation, a portion were allowed to survive and serve as parents. This was done in two ways. First, through "elite" selection, the top 5% of the population was guaranteed survival. In the second scheme, an additional 35% was selected through roulette wheel selection (p_{keep}). The rate of elite selection is kept small to prevent higher performing individuals from swamping the gene pool. p_{keep} is rather arbitrary,[19] but was made large so that low performing individuals would still have a chance to breed and perhaps generate better performing unit cells. To produce offsprings, every surviving individual mated with another survivor until the population size was reached. The second mate in this mating process was selected through roulette wheel selection, so the more fit individuals would generally have more offspring. This process is illustrated in Fig. 3(b).

4. Fitness function design

Each individual is assigned a "fitness score," generated by a fitness function. The role of the fitness function is to measure the performance of the unit cell structures so that they can be easily compared and ranked against one another. This is nearly analogous to the goal function of other optimization algorithms by serving as a value that the algorithm attempts to maximize. The fitness function aims to maximize refractive index, minimize impedance, and maximize bandwidth.

The most straightforward approach to accomplish this task would be to create a function that is a linear combination of these values. However, this could produce negative values, which are not acceptable since roulette selection requires positive values for probabilities. If, instead, a non-linear function is employed, it can be more efficient and yield greater control.[20]

There have been some proposed methodical design procedures for fitness functions, but the design process remains a largely arbitrary and iterative task.[19] Although the fitness function is crucial to the performance of the GA, as long as it penalizes and rewards the individuals properly, numerous different fitness functions will eventually achieve the same solution albeit over many generations.

The main rationale for creating more intelligent and sophisticated fitness functions tends to be for efficiency, i.e., reaching a globally convergent solution with as few iterations as possible. However, this increases the probability of the algorithm settling onto a locally optimal solution instead.[19] For this particular task, since we were only interested in the final solution, efficiency is not a concern. Instead, we took a more conservative approach and constructed a fitness function that attempted to satisfy a few key goals described in more detail in the following.

The primary purpose of this algorithm was to maximize n, the refractive index, so the fitness function was designed to increase exponentially with n. This was preferred over a linear relationship because marginal increases in the maximum achievable refractive index are very valuable, even at the cost of less bandwidth or increased impedance mismatch. For instance, an increase of the refractive index by 150% which incurs a 100% increase in impedance would be desirable. Thus, by exponentiating the refractive index it becomes the most influential variable.

In order to minimize Z, the unit cell's impedance, the fitness function was designed to decrease like a low-pass filter: A smaller impedance value is preferable as long as it was within the regime of 2.0–3.0 (relative to the impedance of the background). But below this range, there are only marginal gains if the Z is minimized more. Further minimization of Z might cause trade-offs with n and the bandwidth. For $Z < 1.2$, the fitness function is designed to exponentially decay with decreasing Z. This is because $Z < 1.2$ typically indicates dispersive behavior such as resonance of the unit cell structure. The exact behavior of the fitness function with respect to impedance can be adjusted by changing the breakpoint ($Z_{\max}$) and the steepness of the transition region (c_3). Therefore, this forces Z minimization to be a secondary concern once Z is minimized past a certain threshold. n then continues to increase unless it causes Z to significantly increase.

Attempting to maximize for the bandwidth of the lens is challenging. Performing an entire frequency sweep is very computationally expensive. The solution employed in this work is to exploit the monotonic frequency response of the impedance. It was observed that Z either monotonically increases or decreases up until a frequency f_c, after which Z remains constant near 0, as we will see later. Therefore, minimizing the absolute value of the slope of the impedance, Z', at 3000 Hz, serves as a good substitute for a frequency sweep. The slope is approximated by sampling Z at 3000 and 3100 Hz. In the edge case where f_c lies between 3000 and 3100 Hz, the calculated slope of Z would be either very dramatic (if Z monotonically increases) or only slightly less than the true slope (if Z monotonically decreases). In contrast, if n were employed instead and f_c were in between the sampling frequencies, the slope of n would have been close to 0 since n does not become 0 above f_c, as we will see later. Thus, Z provided a robust approximation to calculating bandwidth. Unlike Z, Z' in the fitness function decreases without a square root because there was a greater range of "permissible" values the slope could fall under.

One problem encountered with this approach is that when a full frequency sweep was performed on some of the optimized cell structures following these three criteria, the impedance would sometimes suddenly drop off right above 3100 Hz. Therefore, in order to encourage an even more uniform frequency response, the second derivative of impedance was also inspected. Generally, $Z'' \ll Z'$ in all of the simulations. Z'' only becomes significant if it is very large and Z' is large as well. Otherwise Z' dominates in its effect on f_c since both values are both positive or both negative. Therefore, the ratio Z'/Z'' was minimized rather than just Z' because a relatively large Z'' would be permissible as long as Z' is very small. Z'' was found by solving for the impedance at $f = 2950$, 3000, and 3100 Hz. As for the minimization of Z', there is no square root because there is a larger permissible range of values under which the ratio of Z'/Z'' can fall.

Finally, this resulting expression was placed into a logarithm. This ensures that the fitter unit cells will not completely swamp the gene pool so that even in later generations, the GA would still be free to explore unit cell structure variations with initially lower fitness scores. The advantage of this logarithm operator is it expands the search space considerably. The disadvantage of course is that since survival is less strongly correlated with fitness, more generations are needed for convergence to occur.

$$F = \begin{cases} \ln\left[1 + \dfrac{1}{1 + \left(\dfrac{|Z'|}{Z'_{\max}}\right)^{c_1}} \dfrac{1}{1 + \left(\dfrac{Z'}{KZ''}\right)^{c_2}} e^{Zn/2}\right], & Z < 1.2 \\ \ln\left[1 + \dfrac{1}{1 + \left(\dfrac{|Z'|}{Z'_{\max}}\right)^{c_1}} \dfrac{1}{1 + \left(\dfrac{Z'}{KZ''}\right)^{c_2}} \dfrac{e^{1.2n/2}}{\sqrt{1 + \left(\dfrac{Z - 1.2}{Z_{\max} - 1.2}\right)^{c_3}}}\right], & Z \geq 1.2, \end{cases} \tag{1}$$

where $Z' = dZ/df$, $Z'' = d^2Z/df^2$, $Z_{\max} = \text{constant}$, $K = \text{constant}$, and f is the frequency.

This proposed, generalized, fitness function also allows for adjustment of the importance of the variables relatively easily. For example, $Z_{\max}$ and K could be adjusted to shift the fitness function's focus to increasing index, away from optimizing impedance mismatch and broadbandness. This provides further fine-tuning abilities whereby the fitness function is a tool for finding unit cells that match a specific criterion, not just an optimization. If we know what the desired focal distance of a lens is, for instance, we could then calculate the refractive index n_f and manipulate the function to maximize toward $n > n_f$ while minimizing impedance and maximizing broadbandness. This could be particularly useful for other metamaterial applications.

5. Crossover

In GAs, crossover is the operation through which parents combine their chromosomes to create the child chromosomes. The simplest form of crossover is a one-point crossover in which a random index b is selected in the chromosome length, e.g., between 1 and 18, inclusive. All the genes before b are taken from the first parent's chromosome and all the genes up to and after b are taken from the second parent. A two-point crossover generates two indices a and b. Any genes between a and b are taken from the first parent and the rest are taken from the second parent. This allows for more possible child chromosomes and was therefore selected for this study, but one-point crossover should work equally well over many generations.[19] Every child chromosome was generated through crossover.

One deficiency of crossover, particularly when operating with continuous genes, is that it is incapable of introducing new genetic information. A solution employed here is blending. Rather than taking the genes from the first parent exclusively for genes a through b, the genetic information of the two parents are combined in the following way[19]:

$$g_{\text{new}} = \beta g_1 + (1 - \beta) g_2. \tag{2}$$

g_{new} is the new gene, g_1 is the gene from parent one, g_2 is the gene from parent two, and β is an exponential random variable [$\beta \sim \exp(2)$]. This process was repeated, with parents one and two being switched, when performing the rest of crossover over the genes outside of a through b. β was constant over each crossover operation. The blending operator was only applied to the continuous information within the genes, so the flags for shape type and add/sub were combined in the original discrete manner.

6. Mutation

The mutation operator is the primary method through which new genes are introduced into the gene pool. Mutations can occur as either point mutations, i.e., one value in the gene, or a mutation across the entire gene. Both strategies are employed here and hence there are two mutation rates, p_{gene} and p_{point}. Gene mutations generally introduce more change than point mutations. Thus mutations are capable of both large and fine adjustment to the unit cell structure.

Following this scheme, a new gene is generated with probability p_{gene} for every gene whether non-empty or not. For a null gene, no subshape exists at that point so point mutations are impossible. If a gene is present then with probability p_{point}, a random value in the gene will be reassigned a new value by calling the shape generation function. The mutation rates were set high at $p_{gene} = 0.4$ and $p_{point} = 0.18$. High values of mutation were chosen because they encourage additional exploration of the search space, which is particularly helpful in continuous implementations of GAs.[19]

7. Convergence

The algorithm was usually allowed to run until convergence was achieved, which typically took around 500 generations (see Fig. 5). Convergence here was determined to be successful if the best fitness score remained relatively constant for many generations.[19]

This work avoided using techniques designed to improve GA efficiency (faster convergence) such as dynamically manipulating the mutation rate or population size. Such techniques come at the cost of exploring a smaller search space, which makes it more probable to converge on a locally optimal solution. Instead, this paper purposefully attempted to increase the variation of the gene pool and thus explore as much of the search space as possible. This came at the cost of more generations required to reach convergence, but decreased the chance of converging onto a locally optimal solution.

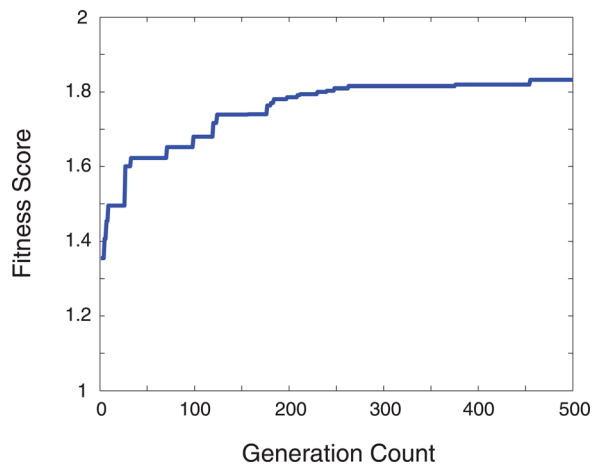

FIG. 5. (Color online) Plot of the best fitness against the generation number. As the generation number increases, the fitness score plateaus, indicating convergence.

The algorithm was run multiple times and achieved similar optimal material parameters each time. Therefore, we are confident that the final optimized material parameters are hard to beat given the considered constraints. It is unlikely that the algorithm, given its broad search space, settled on identical locally optimal solutions each time.

8. Robustness

For simulation robustness, several other functions were introduced to the algorithm. For example, in order to remove unnecessary unit cell structure complexity, a function was created to remove polygons less than 0.35 μm^2 in area from the final structure. Such polygons did not generally significantly alter the results (unless they acted as resonant elements, which decreases bandwidth considerably), but greatly increased the computation time. A different function ensured that the final unit cell was non-empty by forcing mutations until a structure emerged.

III. SIMULATION RESULTS

The physics simulations were all performed in COMSOL MULTIPHYSICS 4.2 with its Acoustics Module and Java API. The server used to run these simulations had 25 Gbytes of memory and utilized an Intel Xeon E5520 processor (4 cores, 8 threads, 8 MB cache, 2.26 GHz, 5.86 GT/s Intel QPI). When the script was run, it would regularly consume 23 Gbytes of memory and utilize all 8 virtual cores by running the simulations in parallel. Each generation would take ~30 min to run because more complex unit cell structures need longer time to simulate. Running the GA over 500 generations took upwards of a week to run.

Figure 6 illustrates two example results attained from the GA. Predictably, decreasing the parameter Z_{max} decreases the maximum n of the GA solution. In addition, increasing the parameter K decreases the bandwidth and Z while increasing n.

It should be noted that at frequencies greater than f_c the value of n is likely physically incorrect. It is difficult to retrieve the correct solution while computing the effective refractive index and impedance from the simulated transmission and reflection coefficients. Fortunately, regions of high dispersion are not useful for metamaterials so it is unnecessary to find the physical solutions in these regions. Most noteworthy was that virtually all the unit cells generated by the GA shared these common features: A "hollow" shape with narrow channels near the x and y axes.

IV. EXPERIMENTAL VERIFICATION

A. Fabrication methods

The results of the GA that were more practically feasible were selected and simplified so that they could be

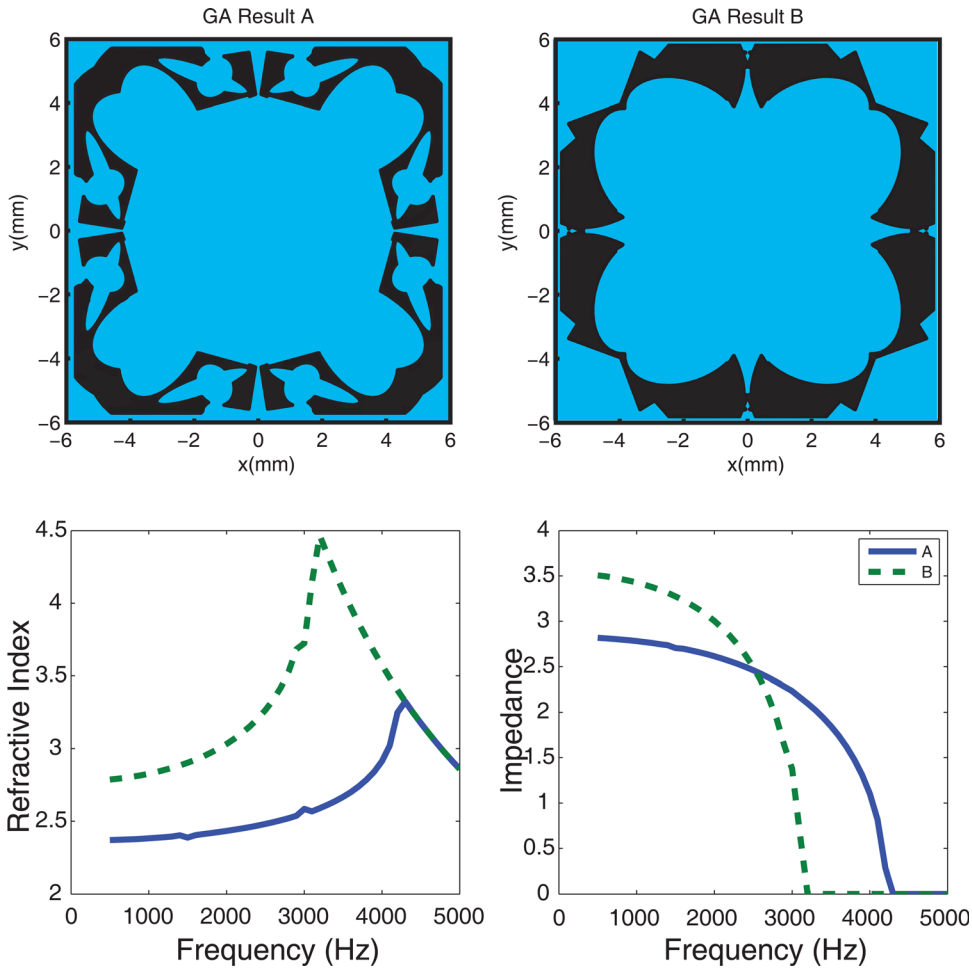

FIG. 6. (Color online) Top: Unit cell structures of two example GA results (black represents the solid structure and the rest represents the air). Bottom: Frequency response of refractive index (left) and impedance (right). The solid line represents the frequency response of GA result A while the dotted line represents the frequency response of GA result B.

realized using a three-dimensional (3D) printer. The goal of the simplification procedure was to create unit cell structures that followed as closely as possible the optimized structures found by the GA. The constraint was that the structures had to fit the resolution of the printer. This method of simplifying the GA results was preferred over modifying the GA itself to create simple forms because doing so would have inherently limited the search space significantly.

Because the waveguide was designed to operate at 3000 Hz, it was unrealistic to increase the operating wavelength in order to allow for scaling of the unit cell size with fewer simplifications.[9] In addition, fabrication costs and size limitations would have made it very difficult to build a larger lens. The fabricated lens was 0.48 m by 0.072 m and required 40 h to print. If instead the lens were to be constructed for 1500 Hz to achieve a twofold increase in precision, the final lens would be 0.96 m by 0.144 m, nearly the same length as the waveguide used for testing the lens (1.2 m by 1.2 m) and would be extremely difficult to construct.

B. Unit cell design

The simplified unit cell structure decided upon for fabrication consisted of a square shell with small inlets at the centers of each of its walls [see Fig. 7(a)]. The optimal thickness of the solid shell was around 0.55 mm in the GA cell of Fig. 6, but this was unrealistic in the fabricated version and was thus set to 1.0 mm, the maximum precision of the 3D printer. The size of the gap present in the solid wall was set to 0.4 mm for similar reasons (this is also why the previously mentioned gap size from Sec. II A between the unit cell structure and waveguide was set to 0.2 mm).

The refractive and impedance mismatch curves over a frequency parameter sweep of Fig. 7 were similar to those in Fig. 6. At 3000 Hz, the refractive index is 2.45 and its impedance is 2.32 as opposed to 2.58 and 2.23, respectively. Thus, the simplification was an effective approximation. Interestingly, during simulation with the simplified unit cell, decreasing the gap size of the channels shifted the f_c toward the target frequency of 3000 Hz and in doing so increased the index while decreasing the impedance.

The best previous design demonstrated experimentally was a unit cell with a structure in the shape of a cross. For this case, the refractive index and impedance for the unit cell in the center were 1.98 and 2.3, respectively.

In addition, the previous design had a greater bandwidth, with f_c of about 5300 Hz as compared to 4300 Hz in the new lens.[11] Thus, this new design sacrifices some bandwidth for an increased refractive index.

Once the geometry of the unit cell placed in the center of the lens has been determined, it is easy to derive the other unit cells toward the extremities of the lens using the following procedure. The size of the narrow inlets in the walls of the unit cell central cavity are kept constant but the size of

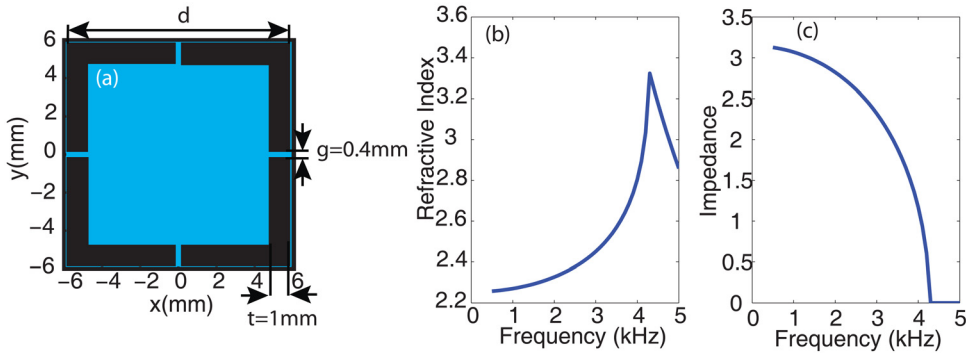

FIG. 7. (Color online) Simplified GA cell design. (a) Geometry of the unit cell; (b) effective index of refraction of the metamaterial generated by the cell; (c) effective impedance.

the cavity (i.e., parameter d in Fig. 7) is reduced in order to achieve the required refractive index profile. This strategy guarantees that the unit cells away from the center of the lens are at least as broadband as the center ones and are characterized by smaller impedances as well. The distribution of the length of the unit cell structure, d, is shown in Fig. 7(a).

C. Lens characterization

It is desirable in numerous applications to work with plane waves. Current technology achieves this by using phased array speakers. However, a simpler and very effective alternative is to use an acoustic lenses instead, placed a focal length away from a point sound source, which can be a regular speaker. We demonstrate this idea in the following.

In order to obtain a wave with a plane front of reasonable extent, the aperture of the lens should be large with respect to the number of wavelengths. It is also advantageous to use a lens with a focal length as small as possible since this is the distance between the collimator and the sound source. The high index of refraction of the metamaterial generated by the unit cell designed previously allows for a GRIN lens whose aperture is four wavelengths (in air), twice the aperture of previous designs.[10,11]

Iterative numerical simulations performed with COMSOL MULTIPHYSICS were used to find the value of this parameter for the other cells that compose the lens. Figure 8(a) shows the variation of d versus the vertical direction, while Fig. 8(b) shows the variation of the effective index of refraction and effective impedance versus the transverse dimension of the lens. Figure 1(b) illustrates this distribution as a temperature map. The lens thickness is set to six cells, i.e., 7.2 cm, that results in a focal length of 11 cm. Note that this focal length is comparable to that of previously reported devices. A photograph of the resulting device is shown in Fig. 8(c).

The performance of the lens is measured inside of a two-dimensional acoustic waveguide composed of two plastic sheets of dimensions 1.2 m by 1.2 m and separated by approximately 5 cm. A 3 in. diameter speaker is used to generate short sound pulses. The pulses were Gaussian and modulated with a sinusoidal signal that had a window of approximately five periods at 3000 Hz.[9] The sound inside the entire waveguide is measured by a microphone moved in steps of 2 cm in both the horizontal and vertical directions. The details of the measurements of the spatial variation of acoustic fields are presented in Ref. 11.

Figure 9 shows the behavior of the newly constructed lens employed as a collimator (left) compared to that of a previous design reported in Ref. 11 (right). Both the sound field amplitude and phase at 3000 Hz are recorded in the region immediately behind the lenses. The larger aperture of new lens (referred here as the "4λ lens") made possible by the higher refractive index in the middle of the lens results in a flatter wave front and a very collimated beam that keeps its Gaussian shape even up to seven wavelengths behind the lens.

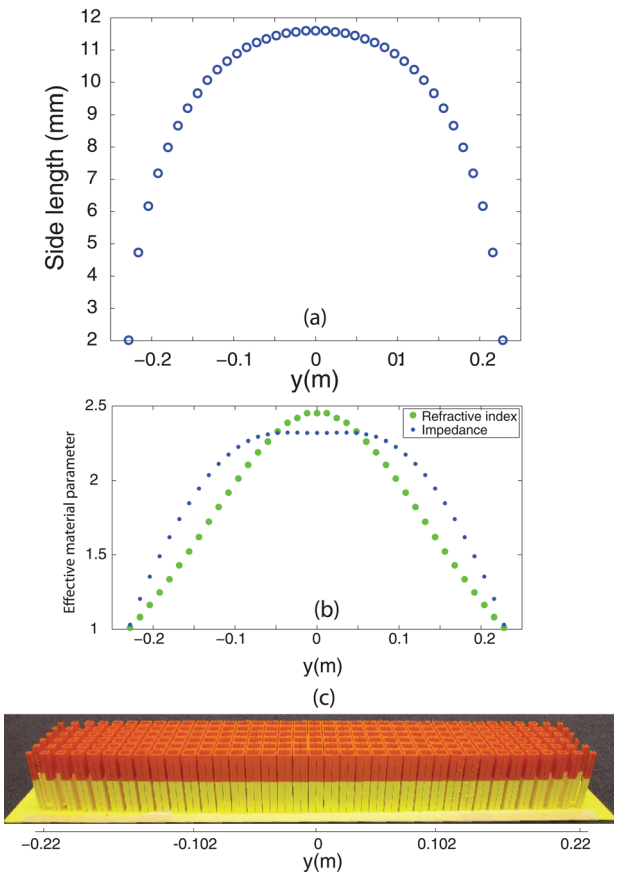

FIG. 8. (Color online) Lens design. (a) Variation of unit cell structure's size, d, in the direction perpendicular to the acoustic axis. (b) Effective refractive index and impedance variation perpendicular to the acoustic axis. (c) Photograph of the lens. Note that the last rows of unit cells are missing on the left/right of the lens because they were too small to support themselves. The difference in color was due to changing the plastic cartridge during the printing process but this has no effect on the lens performance.

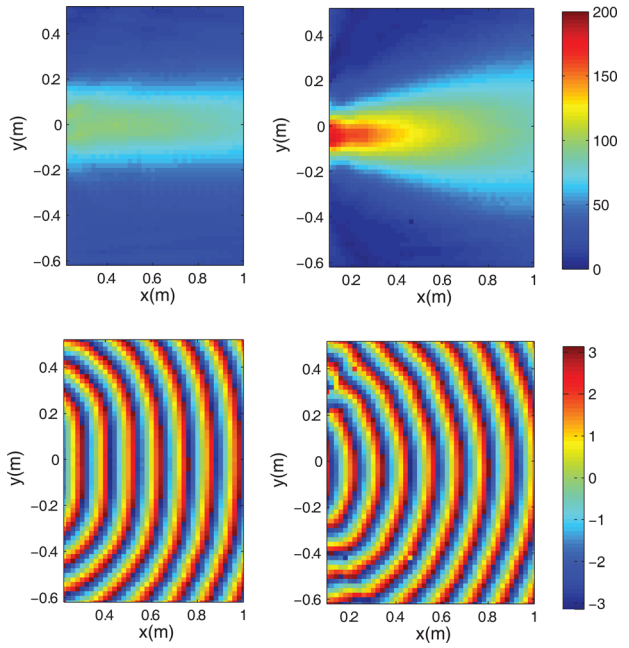

FIG. 9. (Color online) Comparison between frequency domain measurements (top— magnitude; bottom—phase) of lens designed using genetic algorithms (left panels) and lens reported in Ref. 11. The larger lens aperture made possible by the improved cell design makes it a much better collimator than past designs.

Figure 10 illustrates the phase for the two lenses, sampled from a line parallel to the y axis and 24 cm behind the lens. Notice that the curvature of the 4λ lens is much flatter than that of the 2λ lens.

This comparison might seem unfair because of the difference in aperture. The purpose is to emphasize the lens behavior of the new unit cell design and the benefits of a higher refractive index. When trying to build a larger lens, one often encounters the problem that a higher refractive index tends to lead to impedance and fabrication challenges.

However, because of the approach employed here, we were able to achieve a new unit cell design that was characterized by an increased refractive index but retained the same impedance as that of the previous design. This enabled the construction of a larger lens. Had we attempted to construct a lens using the previous unit cell designs, it would have had to be thicker in order to achieve the same focusing ability and thereby suffered from increased reflection. Thus, the improved focusing ability comes from both the larger aperture and the improved unit cell design.

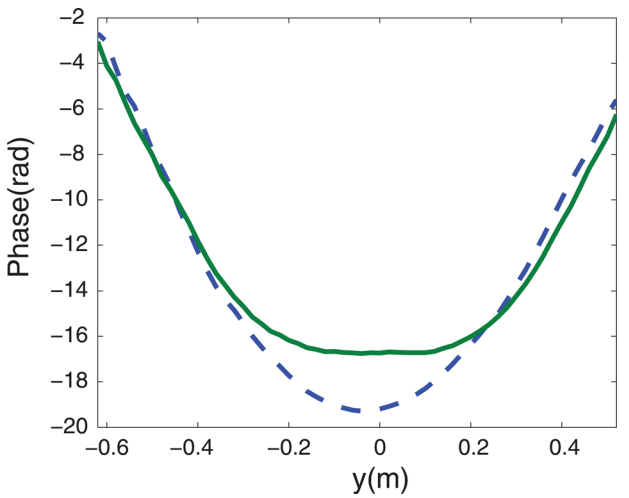

FIG. 10. (Color online) Phase of the pressure measured 0.24 m behind the lens. The dotted line represents the 2λ lens while the solid line represents the 4λ lens.

V. CONCLUSION

In this work, we have implemented and applied a GA approach to optimize the design of an acoustic metamaterial for use as an acoustic lens in air. By placing solid material in the unit cell, the algorithm attempted to maximize refractive index, minimize the lens material acoustic wave impedance, and minimize the frequency dependence of the refractive index and impedance. When these unit cells are used to construct an acoustic lens, these optimizations led to shorter focal lengths, reduced incident wave reflections, and less frequency dependent behavior, respectively. The effective material parameter values that emerged from the GA optimized solutions describe an optimal "landscape" of trade-off between the material parameters.

Some interesting and rather exotic unit cell structures were produced by the GA. Generally, the unit cell structures tended to take on a form of a hollow shape with small gaps. The unit cells had small volumes of solid material, minimizing the effective bulk modulus and thus the acoustic wave impedance. The unit cells also had nearly continuous solid structures with small channels, which create a large effective mass, maximizing the refractive index.

Fabricating the optimized designs proved to be challenging. Therefore, the common features of the optimal unit cells were used to create a simpler unit cell but with n, Z, and a bandwidth close to the initial values. The new design enabled lenses with a larger aperture at a cost of reduced bandwidth.

Although this work focused on the applicability of GAs to unit cell design in acoustic lensing, it can be generalized to any sort of acoustic metamaterial application. In this scheme, the fitness function of the GA employed here can be easily modified to create unit cells that exhibit, as closely as possible, target values for the refractive index, impedance, and bandwidth.

ACKNOWLEDGMENT

This work was supported by a Multidisciplinary University Research Initiative from the Army Research Office (contract no. W911NF-09-1-00539).

[1]R. S. Lakes, T. Lee, A. Bersie, and Y. C. Wang, "Extreme damping in composite materials with negative-stiffness inclusions," Nature (London) **410**, 565–567 (2001).
[2]N. Fang, D. Xi, J. Xu, M. Ambati, W. Srituravanich, C. Sun, and X. Zhang, "Ultrasonic metamaterials with negative modulus," Nature Mater. **5**, 452–456 (2006).
[3]G. W. Milton, M. Briane, and J. R. Willis, "On cloaking for elasticity and physical equations with a transformation invariant form," New J. Phys. **8**, 248 (2006).
[4]D. Torrent and J. Sanchez-Dehesa, "Acoustic cloaking in two dimensions: A feasible approach," New J. Phys. **10**, 063015 (2008).

[5]Y. Cheng, F. Yang, J. Y. Xu, and X. J. Liu, "A multilayer structured acoustic cloak with homogeneous isotropic materials," Appl. Phys. Lett. **92**, 151913 (2008).
[6]J. B. Pendry and J. Li, "An acoustic metafluid: Realizing a broadband acoustic cloak," New J. Phys. **10**, 115032 (2008).
[7]S. Zhang, L. Yin, and N. Fang, "Focusing ultrasound with an acoustic metamaterial network," Phys. Rev. Lett. **102**, 194301 (2009).
[8]B. I. Popa and S. A. Cummer, "Design and characterization of broadband acoustic composite metamaterials," Phys. Rev. B **80**, 174303 (2009).
[9]L. Zigoneanu, B. I. Popa, A. F. Starr, and S. A. Cummer, "Design and measurements of a broadband two-dimensional acoustic metamaterial with anisotropic effective mass density," J. Appl. Phys. **109**, 054906 (2011).
[10]A. Climente, D. Torrent, and J. Sanchez-Dehesa, "Sound focusing by gradient index sonic lenses," Appl. Phys. Lett. **97**, 104103 (2010).
[11]L. Zigoneanu, B. I. Popa, and S. A. Cummer, "Design and measurements of a broadband two-dimensional acoustic lens," Phys. Rev. B **84**, 024305 (2011).
[12]C. Bao, R. Srivastava, C. Gomez-Reino, and M. V. Perez, "Gaussian beam propagation and imaging in hyperbolic secant profile media," Pure Appl. Opt.: J. Eur. Opt. Soc. Part A **5**, 15–27 (1996).
[13]B. I. Popa and S. A. Cummer, "Cloaking with optimized homogeneous anisotropic layers," Phys. Rev. A **79**, 023806 (2009).
[14]V. M. Garcia-Chocano, L. Sanchis, A. Diaz-Rubio, J. Martinez-Pastor, F. Cervera, R. Llopis-Pontiveros, and J. Sanchez-Dehesa, "Acoustic cloak for airborne sound by inverse design," Appl. Phys. Lett. **99**, 074102 (2011).
[15]D. S. Weile and E. Michielssen, "Genetic algorithm optimization applied to electromagnetics: A review," IEEE Trans. Antennas Propag. **45**, 343–353 (1997).
[16]A. Hakansson, J. Sanchez-Dehesa, and L. Sanchis, "Acoustic lens design by genetic algorithms," Phys. Rev. B **70**, 214302 (2004).
[17]V. Fokin, M. Ambati, C. Sun, and X. Zhang, "Method for retrieving effective properties of locally resonant acoustic metamaterials," Phys. Rev. B **76**, 144302 (2007).
[18]J. D. Baena, L. Jelinek, and R. Marqués, "Towards a systematic design of isotropic bulk magnetic metamaterials using the cubic point groups of symmetry," Phys. Rev. B **76**, 245115 (2007).
[19]R. L. Haupt and S. E. Haupt, *Practical Genetic Algorithms* (Wiley, Hoboken, NJ, 2004), pp. 1–25, 95–150, 151–186.
[20]V. Silva, A. da Cruz, E. Carrano, F. Guimaraes, and R. Takahashi, "On nonlinear fitness functions for ranking-based selection," in *Proceedings of the IEEE Congress on Evolutionary Computations* (2006), pp. 305–311.